Real time Method based on SVM for Depth-of-Interaction Identification in PET Scanners

M. Sayed*, A. Arafa, and H. I. Saleh

Radiation Engineering Department, Atomic Energy Authority, EAEA, 3 Ahmed El-Zomar Str., 8th District, Nasr City, Cairo Egypt

ARTICLE INFO

ABSTRACT

Positron Emission Tomography (PET) scanners are based on a ring of scintillation detectors where each detector is comprised of an array of crystals usually coupled to a photosensor. The parallax error is the common error that degrades the spatial resolution of the reconstructed image in the PET scanners. This error resulted from the misidentification of the exact depth-of-interaction (DOI). Phoswich based detector has been used as a solution to accurately identifying the DOI. The pulses emitted from the scintillation crystal layer of this detector are discriminated based on the Pulse Shape Discrimination (PSD) method. In this paper, a high rate merged PSD method which depends on only half-length of the scintillation pulse is proposed to enhance the performance of PET scanners. The frequency transform (discrete cosine transform or discrete sine transform) is merged with the support vector machine (SVM) classifier. The PSD method is verified by discriminating 100 000 scintillation pulses of both LSO and LuYAP crystal. The event rate was 24.5 M events/sec. Therefore, the proposed method realizes a high real-time event rate which nominates it for a ClearPET small animal PET scanner. The discrimination efficiency is kept as 91.36% by merging DST4 with the linear kernel of SVM.

1- INTRODUCTION

Positron Emission Tomography (PET) is an imaging modality that provides in vivo high sensitivity molecular imaging [1]. PET scanner is based on a ring of scintillation detectors. Each detector is comprised of an array of crystals which is usually coupled to a photosensor. The spatial resolution measures the ability of the PET scanner to reproduce the distribution of radioactivity in a patient accurately. The recent practical PET scanners can offer 2 to 4 mm FWHM spatial resolution [2] [3]. Different factors affect the spatial resolution of the PET system such as annihilation photon non-collinearity, and parallax error. The annihilation photon non-collinearity arises, when the angle between the two photons is not equal to 180° exactly. The non-collinearly is increased proportionally with the diameter ring, so to reduce this factor a small doctor size is used in the recent design to reduce the ring diameter [4]. Parallax error occurs due to the lack of information about the Depth of Interaction (DOI) inside the detector of the incoming gamma-photons. This error occurs due to annihilations which are done in off-center positions.

To overcome this error, a huge variety of designs have been developed to determine the DOI accurately.

Different DOI encoding approaches have been presented such as multi-layer crystals (phoswich), multiple crystal photodetector layers, monolithic crystal blocks, and dual ended readout. In the multi-layer crystals approach, the phoswich detector is constructed from two or more different layers of scintillation materials with measurable differences in their scintillation decay times. These scintillation layers are read out by the same photodetector. However, when the photon strikes a layer in the detector, the emission of optical light depends on the scintillation decay time of this layer [5]. Then, a PSD method is used to determine the layer of interaction. In the multiple crystal-photodetector layers, two or more separate layers are coupled individually to their own photodetector [6]. Finally, the Monolithic crystal approach depends on multiple photodetectors with multiple independent readouts attached to a single monolithic crystal [7]. The recent phoswich detectors are doped to achieve a high difference in scintillation light between layers. The number of layers in the phoswich detector in the

presented work is equal to two layers [8]. In this paper, we introduce a high rate PSD method to determine the layer type of the phoswich detector.

Several PSD methods based on time domain analysis have been developed such as rise time, charge integration, and charge comparison. In the rise time method, the time difference between two certain fractions of the pulse is computed to determine the PSD [9]. In the charge integration method, DOI is discriminated based on the ratio between the integration of a certain time period with time delay and without time delay [10]. Finally, in the charge comparison method, the amplitude of a predefined window of pulse time is summed to find the crystal type [11, 12]. On the other hand, in another class of the PSD, the scintillation pulses have been transformed from the time domain to another domain to extract the features of the scintillation pulses. For example, the wavelet was utilized to extract the features of Lutetium Silicate (LSO) and Mixed Lutetium-Yttrium Aluminum Perovskite (LuYAP) scintillation pulses [13]. Then, the t-test classifier was used to identify the crystal type based on wavelet features. Several studies have been used a frequency transformer as a feature extractor for the scintillation pulses. On the other hand, the Zernike moments, which are a sequence of polynomials that are orthogonal on the unit disk, is borrowed to the field of PSD. In this Zernike moments –based method, the order of the two-dimensional Zernike polynomial was ten and the classifier was the Support Vector Machine (SVM) [14].

To speed up the discrimination process, 1D Zernike moments and SVM were merged and implemented using VERTIX-2 FPGA. The event rate was 6.2 M event/sec [15]. The discrimination efficiency based on the 1D Zernike based PSD was 91.4% which is slightly less than efficiency in [14]. The obtained rate is equal to 6.2 M event/sec that computed using all samples of the scintillation pulse (16 samples). Another approach of a merged high rate PSD, the FFT was merged with the SVM in only one phase in [16]. The efficiency in this method was 92.2% and the event rate also was 6.2 M event/sec. Again, all pulse samples were used in this method for discrimination. Thus, the event rate can be accelerated by reducing the number of processed samples from the scintillation pulse provided that; the discrimination efficiency is not decreased significantly.

The main contribution of the proposed work is to merge the feature extractor (DCT or DST) with the classifier (SVM) in one mathematical operation. Then, to reduce the complexity of the proposed PSD method, we will not use all samples of the scintillation pulses in the discrimination process. Thus, the event rate of the PSD methods presented in [15], and [16] can be accelerated

by decreasing the number of samples . Therefore, the proposed method can achieve a higher event rate than was presented in [17]. The proposed method is implemented using Xilinx Zynq-XCZ7010 FPGA to validate the required real time rate.

2- MATHEMATICAL BACKGROUND

2.1 DCT/DST

The basis functions of DSTs and DCTs are eigenvectors for the matrix version of the homogeneous harmonic oscillator system. Each DCT type is constructed from real basis orthogonal vectors whose components are cosines [18]. These vectors are computed from the discretized solutions of the un-damped harmonic oscillator equation $u'' + \lambda u = 0$ (on the domain $x \in [0, \pi]$) with certain homogeneous boundary conditions. By varying the boundary condition type (such as Dirichlet), the different DCT types are obtained [19]. On the other hand, in the DST, the entries of the basis vectors are sines instead of cosines. In this work, we evaluate the performance PSD based on each type of DSTs and DCTs.

The relation between the DCT or DST and the simple harmonic oscillator is an efficient tool in signal processing [20]. The discretization of the simple harmonic oscillator system reflects the reality in which one has to deal with samples, measurements, and time instants [21]. The kernel matrix for each type of the DCT type is computed according to equations 1-a, 1-b, 1-c, and 1-d.

$$\left(DCT\,1\right)_{n,k} = \gamma_k \gamma_n \sqrt{\frac{2}{N-1}} \cos\left(kn\,\frac{\pi}{N-1}\right) \qquad (1-a)$$

$$\left(DCT\,2\right)_{n,k} = \sqrt{\frac{2}{N}}\sigma_k \cos\left(\left(n+\frac{1}{2}\right)\frac{k\,\pi}{N}\right) \qquad (1-b)$$

$$\left(DCT\,3\right)_{n,k} = \sqrt{\frac{2}{N}}\sigma_n \cos\left(\left(k+\frac{1}{2}\right)\frac{n\pi}{N}\right) \qquad (1-c)$$

$$\left(DCT\,4\right)_{n,k} = \sqrt{\frac{2}{N}} \cos\left(\left(k+\frac{1}{2}\right)\left(n+\frac{1}{2}\right)\frac{\pi}{N}\right) \quad (1-d),$$
$$n,k = 0,1,2,....N-1$$

Where N is the number of the coefficients in each transform, k is the coefficient index. And $\gamma, \sigma, \varepsilon$ are scaling factors related to the boundary condition of the harmonic equation. These factors are computed as follows:

$\gamma_n = \frac{1}{\sqrt{2}}$ for n = 0 or N − 1, $\sigma_n = \frac{1}{\sqrt{2}}$ for n = 0, $\varepsilon_n = \frac{1}{\sqrt{2}}$ for n = N − 1

On the other hand, the four kernels of the DST are computed using the following four equations:

$$(DST\,1)_{n,k} = \sqrt{\frac{2}{N}}\,\sin\left(kn\,\frac{\pi}{N}\right), \qquad n,k = 1,2,3,...N-1 \qquad (2-a)$$

$$(DST\,2)_{n,k} = \sqrt{\frac{2}{N}}\varepsilon_k\,\sin\left(\frac{(k+1)\left(n+\frac{1}{2}\right)\pi}{N}\right) \quad n,k = 0,1,...N-1 \qquad (2-b)$$

$$(DST\,3)_{n,k} = \sqrt{\frac{2}{N}}\varepsilon_n\,\sin\left(\frac{\left(k+\frac{1}{2}\right)(n+1)\pi}{N}\right) \quad n,k = 0,1,...N-1 \qquad (2-c)$$

$$(DST\,4)_{n,k} = \sqrt{\frac{2}{N}}\,\sin\left(\frac{\left(k+\frac{1}{2}\right)\left(n+\frac{1}{2}\right)\pi}{N}\right), \quad n,k = 0,1,2,...N-1 \quad (2-d)$$

2.2 Support vector machine (SVM)

SVM is an efficient classifier in DSP due to its ability to classify data accurately [22]. SVM can be used to classify two or more data types. Data are transformed into the required form using the kernel function (such as linear, radial bases function (RBF), or quadratic). The classification is performed in two phases; training and testing phase. In the training phase, the optimal separating hyperplane is determined using the predefined data type. This plane maximizes the margin between two classes of training data points. In the training phase, the validation phase is performed to find the optimal SVM parameters. Then, in the testing phases, the unknown vector (X) can be classified using equation (3). The value of this equation is positive for class one and negative for class two.

$$D(x) = sign(\sum k(X, V_i)\alpha_i y_i + b) \qquad (3)$$

Where k is the kernel function, the α_i's and y_i's are weights depending on the support vector V_i 's, and b is the bias. The linear kernel is defined in equation (4).

$$k(X, V) = X\sigma_i V_i \qquad (4)$$

σ_i is a scale factor for ith feature. The simplification of equation (3) is introduced in the next section where the simplified equation is implemented to perform the real-time discrimination.

3- The Proposed Merged DCT/DST-SVM PSD method

The proposed method is based on merging the DCT/DST and SVM in one phase. To accelerate the PSD rate, a segment from the scintillation pulse is used in discrimination. The feature extractor in the proposed work uses on only one type of the DCTs or DSTs and the SVM is used as a classifier.

The data set of scintillation pulses is divided into two data subsets; training subset and testing subset. To classify the scintillation pulses, the proposed method was applied to the scintillation pulses in two phases; the training and the testing phase. In the training phase, the pulses of the training subset were transformed based on only one type of DCT or DST as illustrated in equation (1), or (2) respectively. Then, the SVM was applied to the frequency components to find the following parameters; support vectors, the base, and the scale factor. However, the training phase was performed offline to calculate the SVM parameters. Finally, we formulated the discrimination-vector ($\mathbf{Sf_0, Sf_1, ...}$) according to the equations (6) and (7). Then, the discrimination of the unknown pulses is performed using only equation (5).

The decision function ($\mathbf{D}$) which classify the unknown pulse ($\mathbf{p}$) with ($\mathbf{N}$) samples is defined as in[16] :

$$D(\mathbf{p_0}) = sign\left[(\mathbf{p_0} \quad .....\mathbf{p_N})\begin{pmatrix} sf_0 \\ \vdots \\ sf_{N-1} \end{pmatrix} + \mathbf{b}\right] \qquad (5)$$

$\mathbf{Sf}$ is defined as :

$$\mathbf{Sf_{N\times1}} = (\mathbf{T_{N\times N}}) * (\mathbf{\sigma_{N\times1}} \quad . \quad (\mathbf{S_{N\times L}} * \mathbf{\alpha_{L\times1}})) \qquad (6)$$

Where ($\mathbf{T_{N\times N}}$) is the transformation kernel of DCT or DST with $\mathbf{N}$ frequency components, $\mathbf{S_{N\times L}}$ is the support vector, $\mathbf{\alpha}$ is the weight of the feature, and $\mathbf{\sigma}$ is the scale factor, and L is the number of support vectors as explained before.

The elements of the ($\mathbf{Sf}$) matrix are computed as follows:

$$Sf_n = \begin{pmatrix} f_{n,0} & \cdots f_{n,N-1} \end{pmatrix} \begin{bmatrix} \sigma_0 \sum_{l=0}^{L-1} S_{o,l} y_l \alpha_l \\ \vdots \\ \sigma_{N-1} \sum_{l=0}^{L-1} S_{N-1,l} y_l \alpha_l \end{bmatrix} \quad (7)$$

Where $f's$ are the elements of the transformations matrix T of DCT or DST, and n= 0,1,2,....,N-1. The parameters of the SVM which are the hyperplane, support vectors, the base, and the scale factor, are optimized using the quadratic programming function of MATLAB.

The proposed method is shown in figure 1. The testing phase is performed offline to find the parameters of the SVM. While in the testing phase, the tested pulses are discriminated in real time according to only equation(5).

The discrimination of efficiency of the proposed method is computed according to the equation (8).

$$\text{Total efficiency (\%)} = \left(\frac{\text{correct LSO pulses+correct LuYAP pulses}}{\text{total number of LSO and LuYAP pulses}} \right) \times 100 \quad (8)$$

While the prediction efficiency of LSO and LuYAP types are given by the following equations:

$$\text{LSO pulses efficiency} = \frac{LSOtrue}{LSOtrue+LuYAPfalse} \quad (9)$$

$$\text{LuYAP pulses efficiency} = \frac{LuYAPtrue}{LuYAPtrue+LSOfalse} \quad (10)$$

On the other hand, the errors in prediction for the two types of pulses are given by equation (11, 12).:

$$\text{LSO pulses error} = \frac{LuYAPfalse}{LSOtrue+LuYAPfalse} \quad (11)$$

$$\text{LuYAP pulses error} = \frac{LSOfalse}{LuYAPtrue+LSOfalse} \quad (12)$$

The complexity of the testing phase of the PSD based on DCT/DST and SVM is $N^2 + NM$ multiplications for N samples scintillation pulse and M in number support vectors. This complexity is estimated based on calculations both of the transformation and classification steps are performed separately. The complexity presented in [15] was (N) multiplications and ($N + 1$). The complexity of computations can be reduced where segment of pulses was used in the discrimination process. Besides, the discrimination efficiency of the proposed method is still in an acceptable range (the variation in discrimination efficiency between using all or half samples of the pulse in discrimination is discussed in section 4-3).

On the other hand, we computed the Figure of merit (FOM) according to next equation [23] for the DCT/DST coefficients, to study the overlap between coefficients:

$$FOM = \frac{LSO\ peak-LuYAP\ peak}{FWHM\ of\ LSO-FWHM\ of\ LuYAP} \quad (13)$$

To perform the real time processing of the scintillation pulses First-In First-Out memories (FIFOs) have been used to read the scintillation pulses. Where, these memories are used as a buffer to synchronize the pulses of the readout system of the detector with the FPGA. Based on this concept, the interface between the different speed components of the proposed work can be implemented without any loss in the scintillation pulses. Otherwise, the huge pulses of the scintillation decorator will be lost due to miss match between the different parts of the system [24].
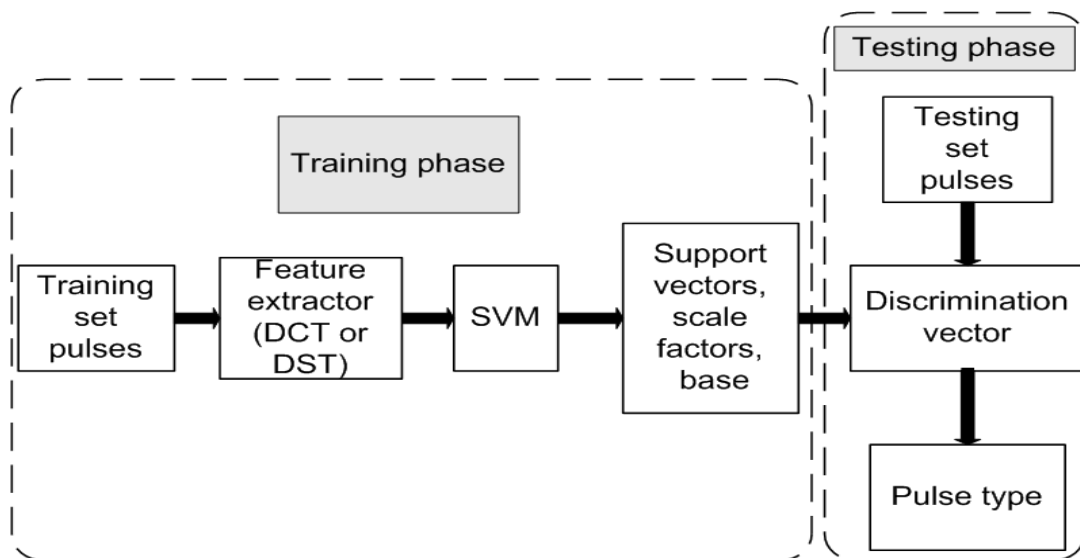

Fig. (1): The offline training and the online testing phase.

4- EXPERIMENTAL RESULTS AND DISCUSSION

To verify the proposed method, it is applied to a data set of LSO and LuYAP pulses. These pulses were recorded in ZEL, Juelich [25-27] . The data set of 100 000 pulses was recorded, 50 000 for each type. The covering time window was 400 ns thus each scintillation pulse is represented by 16 samples.

The scintillation pulses of the LSO and LuYAP are discriminated based on the proposed method. Two pulses for LSO and LuYAP are represented in figure (2). The proposed method is performed using MATLAB software. The data set is divided into three data subsets; training, validation, and testing. The training data subset is 2000 pulses from each type. On the other hand, the validation data subset (1000 pulses for each type) is used in the optimization of the parameters of the SVM, and the quadratic programming model in MATLAB is used in this optimization. The testing data subset is 47000 pulses for each type.
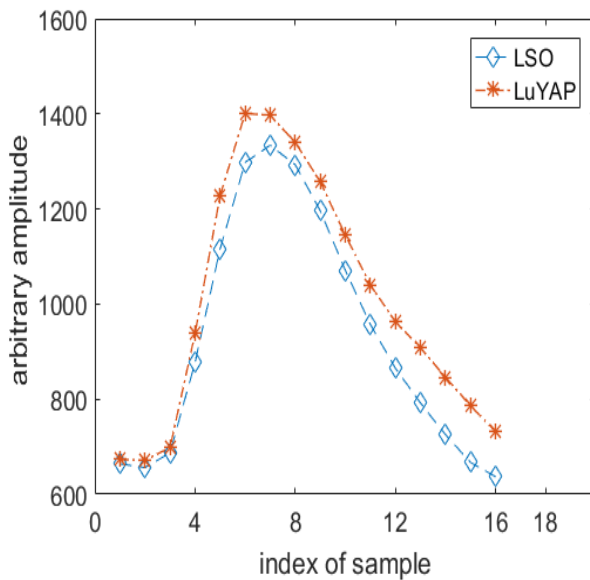

Fig. (2): The original pulse of LSO and LuYAP crystals.

Figure 3 shows the percentages of the discrimination efficiency for the proposed method using different types of the DCT/DST. The discrimination using DST4 is the best, which equals to 92.54% as represented in figure 3.

All samples of pulse were used in this computation to compare between the discrimination efficiency based on all samples and segment of pulses as we proposed. This figure shows a small difference between the discrimination efficiencies using the proposed types. A possible explanation for these differences might be that the changes in histogram between the frequency coefficients is small in all types (i.e. there is no type has a significant difference between coefficients). Figure 4 and figure 5 show the mean and standard deviation of the DCT and DST coefficients respectively. The amplitude of high frequency is very small due to the filtration of the pulses using the LPF as mentioned before.

To determine the overlap between different frequency coefficients, the FOM was computed for each coefficient according to equation (15). Where, we transformed the scintillation pulse (16 samples) and each coefficient was determined. Table 1 illustrates the FOM for each coefficient of the DCT/DST types. The FOM values were very small, due to the overlap between the coefficients as shown in figures 4, and 5.
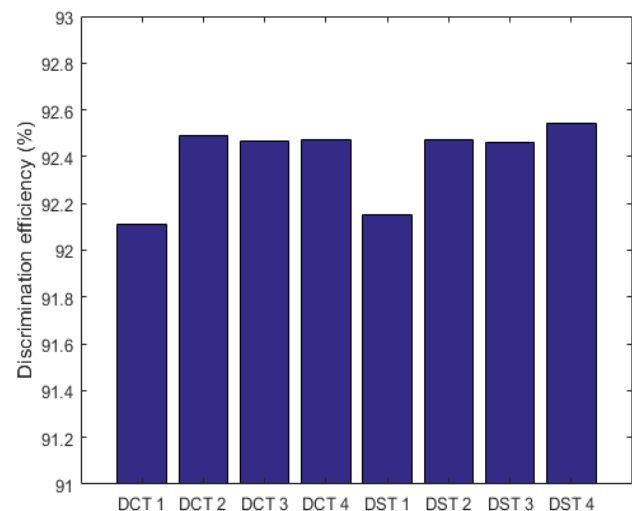
Fig (3): The percentages of the discrimination efficiency for the proposed method using DCT1, DCT2, DCT3, DCT4, DST1, DST2, DST3, and DST4.
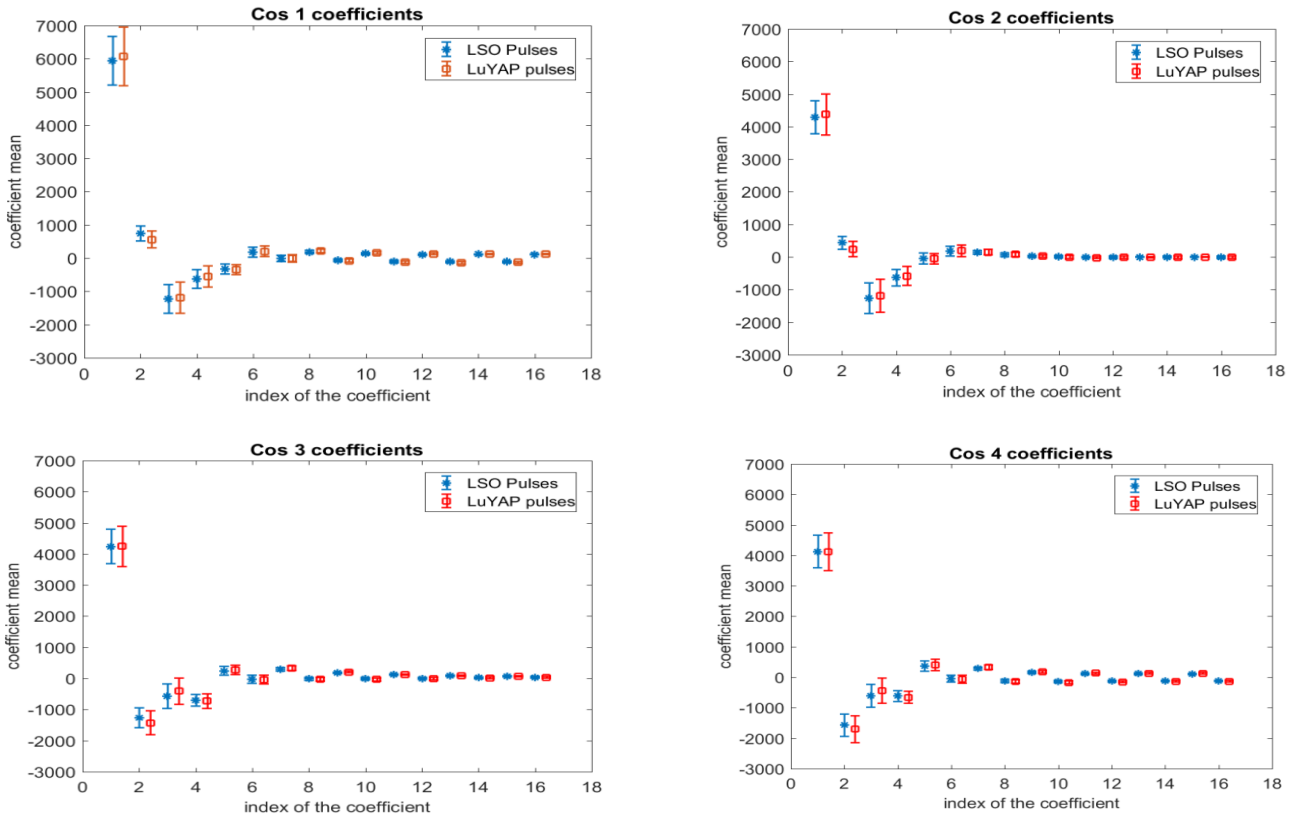
Fig. (4): Mean and standard deviation of the sixteen coefficients for all DCT types (DCT1, DCT2, DCT3, and DCT4) which computed form the two types of pluses (LSO And LuYAP)
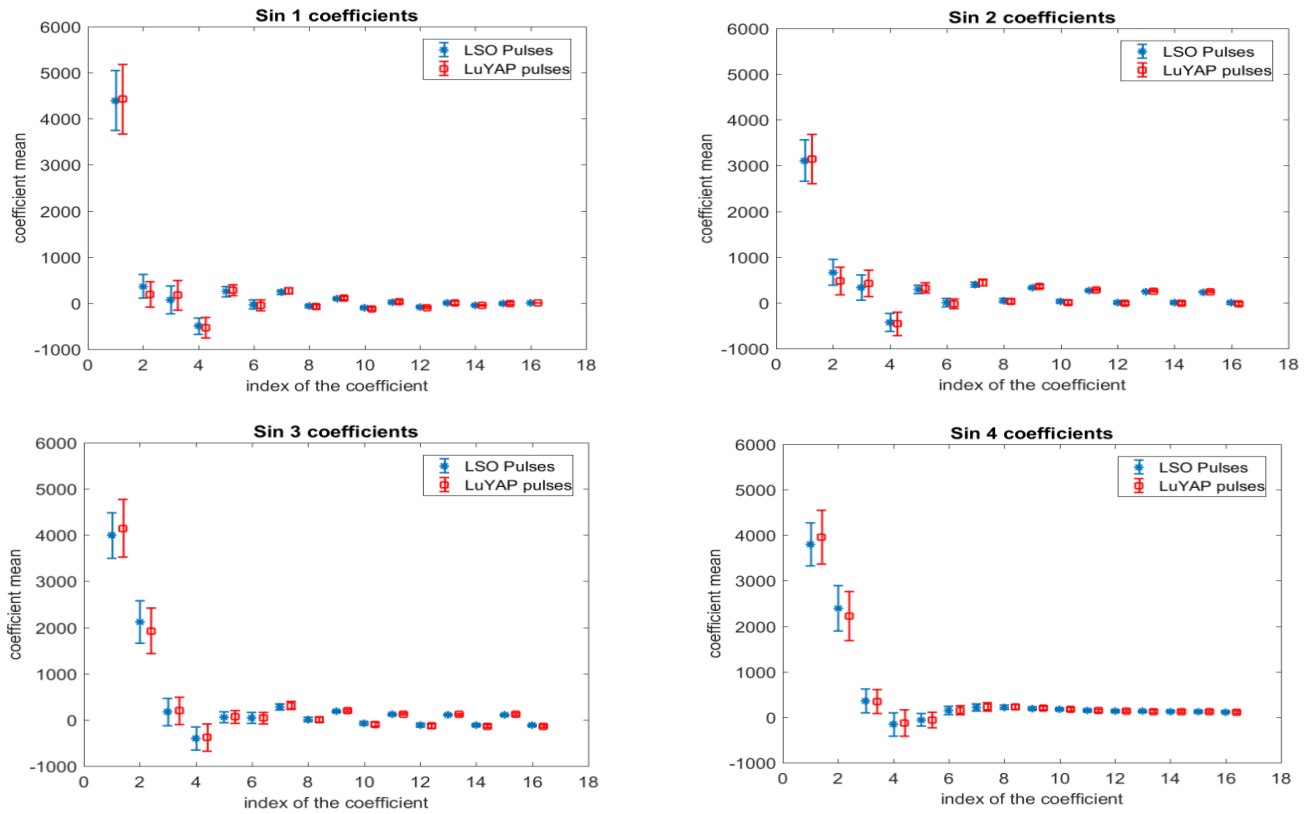
Fig. (5): Mean and standard deviation of the sixteen coefficients for all DST types (DST1, DST2, DST3, and DST4) which computed form the two types of pluses (LSO And LuYAP)

Table (1): The FOM of all DCT/DST coefficients of the studied pulses

Coefficient index	DCT1	DCT2	DCT3	DCT4	DST1	DST2	DST3	DST4
1	0.1178	0.0708	0.0714	0.0135	0.0319	0.0018	0.1414	0.0966
2	0.2391	0.226	0.1094	0.1021	0.2667	0.2032	0.1269	0.0931
3	0.0633	0.0998	0.1656	0.0706	0.1665	0.0154	0.0285	0.017
4	0.1261	0.0032	0.0873	0.0829	0.0493	0.122	0.0401	0.0198
5	0.0014	0.1071	0.0005	0.072	0.0883	0.1675	0.0263	0.1151
6	0.0638	0.0444	0.0555	0.1462	0.0698	0.0559	0.0002	0.0452
7	0.0817	0.023	0.0758	0.2209	0.0377	0.1349	0.0907	0.0012
8	0.0882	0.0061	0.1372	0.1329	0.017	0.1507	0.1135	0.0679
9	0.017	0.0583	0.2106	0.0625	0.0961	0.0982	0.2021	0.0088
10	0.1781	0.0261	0.1487	0.2035	0.0978	0.2006	0.0868	0.0517
11	0.1544	0.0043	0.0433	0.2075	0.1467	0.1647	0.0085	0.0179
12	0.152	0.0943	0.2413	0.2497	0.0143	0.2306	0.1557	0.0207
13	0.2239	0.1163	0.1348	0.2763	0.0349	0.2572	0.2092	0.0177
14	0.3511	0.0044	0.1048	0.1363	0.165	0.2942	0.2744	0.0484
15	0.2631	0.1315	0.0974	0.2007	0.0416	0.2574	0.2475	0.0526
16	0.1784	0.0825	0.0687	0.5149	0.1168	0.2989	0.3413	0.0211

However, DST4 gives the highest discrimination efficiency as shown in figure 3. In table 2, the discrimination is computed using a number of samples starting from the last two samples, the last four samples... up to all samples of the pulse (16 samples). The discrimination efficiency is a direct proportion to the number of samples. However, we propose to transform only half of the pulse (8 samples) to enhance the event rate (as mentioned before) with a small decrease in efficiency (about 1.2%). Where, efficiencies for all samples of pulses and half samples are 92.54%, and 91.36% respectively. On the other hand, to get a high efficiency regardless of the event rate all samples of pulses are used. Thus, the computation complexity of the merged DST4-SVM PSD method is (N/2) multiplications and (N/2+1) additions if only half of the pulse are used in discrimination. Finally, the merged DST4-SVM PSD method with a linear kernel was implemented on Xilinx Zynq-XCZ7010 FPGA using only half of pulse to achieve the event rate equals to 24.5 M events/sec. Besides, the discrimination efficiency is equal to 91.36% which can be accepted. On the other hand, the rate using all samples of the scintillation pulses is 12.25M events/sec.

Table (2): Efficiency of the proposed linear kernel using the DST4 of number of coefficients based on transform number of samples ranges from 2 samples up to 16 samples

Number of used coefficients of DST4	Efficiency (%)
2	89.12
4	89.64
6	91.31
8	91.36
10	91.59
12	91.76
14	92.26
16	92.54

The error analysis of DST4 using 16 coefficients in discrimination are computed for each type of pulses and illustrated in the table (3). The LSO prediction error is lower than that of LuYAP.

Table (3): Efficiency and error of the proposed method using DST4 of each type pulses according to equations (9-12) for 47000 pulses from each type of pulses

	Predicted LSO	Predicted LuYAP	Error %
Tested LSO	**44729**	4737	4.9%
Tested LuYAP	2271	**42262**	10.1%
Efficiency (%)	95.1%	89.9%	

Table 4, and 5 represent the device utilization summary and timing report of the proposed work using Xilinx Zynq-XCZ7010 FPGA. The number of the slice register and the lookup tables (LUT) are very low where the total registers and LUT of the selected FPGA board are 35200, 17600 respectively. Hence a different channel can be processed provided that a suitable FIFO memory is used. On the other hand the minimum period is 5.088 ns thus the maximum frequency is 196.530MHz for each sample from the pulse. Therefore, according to the processed number of the samples in the discrimination, the discrimination speed can be modified of calculation.

Table (4): Device utilization summary

Number of Slice Registers	46
Number of Slice LUTs	105
Number of IOs	23

Table (5): Timing reports (ns)

Minimum period	5.088
Minimum input arrival time before clock	4.432
Maximum output required time after clock	0.848

The main idea of the proposed method is based on merging the feature extractor with a classifier and using a segment of pulses. From the discussed results, the event rate of the proposed method is 24.5 M event/sec where only half of the scintillation pulse (8 samples) is used in discrimination. The DST4-based PSD gives the highest efficiencies for all samples of pulses and eight samples of pulses are 92.54%, and 91.54% respectively. This method is computed using a simplified equation (5) which implemented using Xilinx Zynq-XCZ7010 FPGA. The proposed method is very simple which needs only N/2 multiplications and N/2+1 additions.

Four detectors arrays can share one FPGA chip. The SVM training phase is offline computed in MATLAB software to get the support vector (8 coefficients). These support vectors are multiplied and accumulated with the half pulse vector (8 samples) according to equation (5) and the product is added to the bias (b). The MSB (sign bit) of the final value decides the type of the pulse; 0 for LuYAP and 1 for LSO type. Therefore, there is no need to implement the SVM approach in the FPGA.

5- CONCLUSION

A merged PSD method was proposed using DST and SVM. The discrimination is based on only one vector multiplication thus the event rate was enhanced. Where, half samples of each pulse were multiplied with the predefined discrimination vector to identify the pulse type. Different types of DCT and DST were tested to study the effect of different frequency components on discrimination. DST4 provides the best discrimination efficiency (91.36%) based on only half samples of the pulse (8 samples). The event rate based on the proposed merged method can achieve a rate of 24.5.4M event/sec using Xilinx Zynq-XCZ7010 FPGA. Moreover, the presented PSD method might help to implement the discrimination of a large number of detectors pulses on a single chip depending on the FPGA chip size.

REFERENCES

[1] Judenhofer, M.S. and S.R. Cherry. *Applications for preclinical PET/MRI*. in *Seminars in nuclear medicine*. 2013. Elsevier.

[2] Lee, J.S. and J.H. Kim. *Recent advances in hybrid molecular imaging systems*. in *Seminars in musculoskeletal radiology*. 2014. Thieme Medical Publishers.

[3] Van Sluis, J., et al., *Performance characteristics of the digital Biograph Vision PET/CT system.* Journal of Nuclear Medicine, 2019. **60**(7): p. 1031-1036.

[4] Mohammadi, I., et al., *Minimization of parallax error in positron emission tomography using depth of interaction capable detectors: methods and apparatus.* Biomedical Physics & Engineering Express, 2019. **5**(6): p. 062001.

[5] Gu, Z., et al., *A DOI detector with crystal scatter identification capability for high sensitivity and high spatial resolution PET imaging*. IEEE transactions on nuclear science, 2015. **62**(3): p. 740-747.

[6] Berg, E.J., *Detectors, Algorithms, and Scanner Technology for Total-Body PET*. 2016: University of California, Davis.

[7] Müller, F., et al., *A novel DOI positioning algorithm for monolithic scintillator crystals in*

PET based on gradient tree boosting. IEEE Transactions on Radiation and Plasma Medical Sciences, 2018. **3**(4): p. 465-474.

[8] Wei, Q., et al., *A side-by-side LYSO/GAGG phoswich detector aiming for SPECT imaging.* Nuclear Instruments and Methods in Physics Research Section A: Accelerators, Spectrometers, Detectors and Associated Equipment, 2020. **953**: p. 163242.

[9] Wiener, R.I., S. Surti, and J.S. Karp, *DOI Determination by Rise Time Discrimination in Single-Ended Readout for TOF PET Imaging.* IEEE Transactions on Nuclear Science, 2013. **60**(3): p. 1478-1486.

[10] Chang, C.-M., J.W. Cates, and C.S. Levin, *Time-over-threshold for pulse shape discrimination in a time-of-flight phoswich PET detector.* Physics in Medicine & Biology, 2016. **62**(1): p. 258.

[11] Chandrikamohan, P. and T.A. DeVol, *Comparison of Pulse Shape Discrimination Methods for Phoswich and CsI:Tl Detectors.* IEEE Transactions on Nuclear Science, 2007. **54**(2): p. 398-403.

[12] Roncali, E., et al., *Pulse shape discrimination and classification methods for continuous depth of interaction encoding PET detectors.* Physics in Medicine & Biology, 2012. **57**(20): p. 6571.

[13] Arafa, A., et al. *FFT-and DWT-based FPGA realization of pulse shape discrimination in PET system.* in *2009 4th International Conference on Design & Technology of Integrated Systems in Nanoscal Era.* 2009. IEEE.

[14] Arafa, A., H. Saleh, and M. Ashour, *A zernike moment method for pulse shape discrimination in PMT-based PET detectors.* IEEE Transactions on Nuclear Science, 2013. **60**(3): p. 1518-1526.

[15] Arafa, A. and H. Saleh, *A real-time scintillation crystal identification method and ITS FPGA implementation.* IEEE Transactions on Nuclear Science, 2014. **61**(5): p. 2439-2445.

[16] Saleh, H. and A. Arafa, *Real time depth of interaction determination based on Fourier Transform and Support Vector Machine.* Nuclear Instruments and Methods in Physics Research Section A: Accelerators, Spectrometers, Detectors and Associated Equipment, 2017. **872**: p. 74-79.

[17] Streun, M., et al., *The data acquisition system of ClearPET neuro-a small animal PET scanner.* IEEE Transactions on Nuclear Science, 2006. **53**(3): p. 700-703.

[18] Ahmed, N. and K.R. Rao, *Orthogonal transforms for digital signal processing.* 2012: Springer Science & Business Media.

[19] Strang, G., *The discrete cosine transform.* SIAM review, 1999. **41**(1): p. 135-147.

[20] Masera, M., et al. *A novel framework for designing directional linear transforms with application to video compression.* in *ICASSP 2019-2019 IEEE International Conference on Acoustics, Speech and Signal Processing (ICASSP).* 2019. IEEE.

[21] Britanak, V., P.C. Yip, and K.R. Rao, *Discrete cosine and sine transforms: general properties, fast algorithms and integer approximations.* 2010: Elsevier.

[22] Awad, M. and R. Khanna, *Support Vector Machines for Classification,* in *Efficient Learning Machines: Theories, Concepts, and Applications for Engineers and System Designers,* M. Awad and R. Khanna, Editors. 2015, Apress: Berkeley, CA. p. 39-66.

[23] Langeveld, W.G., et al., *Pulse shape discrimination algorithms, figures of merit, and gamma-rejection for liquid and solid scintillators.* IEEE Transactions on Nuclear Science, 2017. **64**(7): p. 1801-1809.

[24] Gordon-Ross, A., S. Abdel-Hafeez, and M.H. Alsafrjalni. *A One-Cycle FIFO Buffer for Memory Management Units in Manycore Systems.* in *2019 IEEE Computer Society Annual Symposium on VLSI (ISVLSI).* 2019. IEEE.

[25] Streun, M., et al., *Pulse shape discrimination of LSO and LuYAP scintillators for depth of interaction detection in PET.* IEEE Transactions on Nuclear Science, 2003. **50**(3): p. 344-347.

[26] Saleh, H., et al. *Efficient FPGA-based multistage two-path decimation filter for noise thermometer.* in *ICM 2001 Proceedings. The 13th International Conference on Microelectronics.* 2001. IEEE.

[27] Streun, M., et al., *Pulse recording by free-running sampling.* IEEE transactions on nuclear science, 2001. **48**(3): p. 524-526.